

**REACTION
ENGINEERING
INTERNATIONAL**

Committed Individuals Solving Challenging Problems

**NUMERICAL PREDICTIONS OF DEPOSITION WITH
A PARTICLE CLOUD TRACKING TECHNIQUE**

by

**James R. Valentine
Reaction Engineering International**

**Philip J. Smith
Department of Chemical and Fuels Engineering
University of Utah**

In this report we describe a model for predicting particle deposition in turbulent flow fields that has been coupled with a particle cloud tracking technique. Through comparison of numerical predictions with experiment data for circular tubes, the method is shown to reasonably predict both isothermal and thermophoretic particle deposition. Although the test cases have been circular tubes, the method is applicable to arbitrary geometries.

Introduction

Deposition of particles from a turbulent flow field onto adjacent walls is an important consideration in engineering applications such as coal combustion, atmospheric pollution, and the design of air cleaning devices. Mechanisms inducing deposition include turbulent diffusion, Brownian diffusion (for very small particles), and external forces such as the thermophoretic force resulting from a temperature gradient. In this study, deposition theory is incorporated into a particle cloud tracking technique and the results are compared to experimental measurements.

The dispersed phase of fluid/particle or fluid/droplet two-phase flows can be modeled by either of two techniques. In an Eulerian technique, the dispersed phase is viewed as a continuum and is modeled with conservation equations similar to those governing the fluid motion. In a Lagrangian technique, discrete particle trajectories are calculated. In either case, interphase coupling is accomplished by the inclusion of source terms in the appropriate conservation equations. Eulerian methods are most applicable to densely loaded systems where particle-particle interactions are a consideration. Lagrangian methods, on the other hand, are well suited for lightly loaded systems where the rarity of particle-particle interactions precludes rendering the dispersed phase as a continuum. Lagrangian methods also provide for particle history effects in reaction considerations.

In cases where turbulent particle dispersion is important, traditional Lagrangian tracking techniques such as the Stochastic Separated Flow model (Shuen, Chen, and Faeth, 1983) which involve Monte Carlo averaging are often used. However, to insure the calculation of smooth interphase source terms and convergence of the two phase flow field, the calculation of unreasonably large numbers of individual trajectories may be necessary, thus these traditional methods often become unwieldy. A newer and more efficient technique involves the tracking of particle clouds or the statistics of ensembles of individual particles (Baxter, 1989 and Jain, 1996). With this method, far fewer trajectories need be determined for calculation of smooth source terms.

Particle Cloud Tracking Technique

A particle cloud or an ensemble of particles is characterized by a mean position and a variance. All particles within the cloud at a given mean residence time are assumed to share the same physical characteristics such as velocity, diameter, composition, and temperature. The mean or expected value for the cloud position, $\langle x_i(t) \rangle$, can be computed from the ensemble averaged particle velocity $\langle V_i(t) \rangle$:

$$\mu_i(t) \equiv \langle x_i(t) \rangle = \int_0^t \langle V_i(\tau) \rangle d\tau + \langle x_i(0) \rangle \quad (1)$$

The angle brackets, $\langle \rangle$, indicate ensemble averaged properties. In the applications of interest here, the only significant forces on the particle are steady state aerodynamic drag and gravity. Thus the motion of the mean position of the cloud is governed by

$$\frac{d\langle V_i \rangle}{dt} = \beta(\langle U_i \rangle - \langle V_i \rangle) + \left(1 - \frac{\rho_f}{\rho_p}\right)g_i \quad (2)$$

where U_i and V_i and ρ_f and ρ_p are the fluid and particle velocities and densities, respectively, and g_i is the component of acceleration due to gravity. The coefficient β in Eq. 2 is given by

$$\beta = \frac{3C_D \rho_f}{4d_p \rho_p} |\langle U \rangle - \langle V \rangle| \quad (3)$$

where d_p is the particle diameter. The drag coefficient, C_D , in Eq. 3 is given by (Wallis, 1969)

$$C_D = \frac{24}{Re_p} (1 + 0.15 Re_p^{0.687}) \quad (4)$$

and the particle Reynolds number in Eq. 4 by

$$Re_p = \frac{\rho_f d_p |\langle \ddot{U} \rangle - \langle \ddot{V} \rangle|}{\mu_f} \quad (5)$$

Thus first moment of the particle cloud positional probability distribution function (pdf), $\mu_i(t)$, (the expected value of the mean particle cloud position) can be computed.

Dispersion of the cloud is described by the second moment or the variance of the cloud positional pdf,

$$\sigma_{ij}(t) = 2 \int_0^t (t - \tau) R_{ij}^p(\tau) d\tau \quad (6)$$

where the particle velocity correlation tensor is given in terms of the fluctuating particle velocity as

$$R_{ij}^p(\tau) = \langle v'_i(t) v'_j(t + \tau) \rangle. \quad (7)$$

The method used to determine $R_{ij}^p(\tau)$ has been developed by Wang (1990) and the current implementation has been described by Jain (1996). $R_{ij}^p(\tau)$ provides an indication of the degree to which fluctuations in the particle position are correlated as the particle is convected. The off-diagonal elements of R_{ij}^p where $i \neq j$ are neglected, leaving two components of R_{ij}^p to be calculated; one in the direction of the drift velocity and one in the transverse direction. Approximations for these gas phase turbulence properties are computed in terms of parameters input from the κ - ϵ gas turbulence model. Particle inertia effects resulting from variations in particle size and density and drift velocity effects are accounted for. Predictions of particle dispersions compare well with experimental measurements (Jain 1996).

Eulerian particle properties are determined through consideration of the weight within a computational cell of the Gaussian pdf with mean and variance given by Eq. 2 and Eq. 6 respectively and the residence time of the cloud within that cell. Ensemble averaged fluid properties are calculated by

averaging the fluid properties in each cell according to the weight of the cloud as determined by Eq. 6 in that cell. To complete the two-phase flow scheme, interphase coupling is accomplished through a particle-source-in-cell technique (Crowe et. al, 1977).

Deposition Model

Particles or droplets transported in a turbulent flow stream can diffuse to an adjacent surface and be deposited through several mechanisms. Brownian diffusion may be important for very small particles, while larger particles may be deposited through inertial effects after becoming entrained in turbulent eddies. External forces such as thermophoresis and electrophoresis resulting from the presence of thermal gradients or electric fields may also affect migration to and deposition on the surface. In the present study we are concerned with deposition through Brownian diffusion, inertial effects, and thermophoresis.

The boundary layer adjacent to a wall is categorized by three regions, the relatively thin viscous sublayer immediately adjacent to the surface and extending in wall coordinates to approximately $y^+ = 6$, the buffer region extending from the edge of the viscous sublayer to $y^+ = 30$, and the log law region beginning at the edge of the buffer region. Turbulent eddy motion extends through the buffer region, but flow in the viscous sublayer is assumed to be primarily parallel to the wall and devoid of eddy motion. The deposition model presented here is based on the theory of Friedlander and Johnstone (1957).

Particles are assumed to diffuse through the buffer region due to turbulent fluctuations of the carrier gas, but impact the surface and are deposited only if they penetrate the viscous sublayer. Large particles may have sufficient inertia to be carried through the viscous sublayer, while small particles may reach the surface only through the action of Brownian diffusion or thermophoresis. To model deposition, it is necessary to model the diffusion of particles through the buffer region and the penetration of particles through the viscous sublayer.

The distance that a particle having an initial velocity of V_0 will travel in a quiescent fluid due to its inertia is defined as the stop distance. Thus, a particle diffusing to one stop distance from the wall is assumed to have sufficient inertia to penetrate the viscous sublayer and reach the wall. The stop distance can be calculated as

$$S = V_0 \tau_p \quad (8)$$

where τ_p is the particle relaxation time, given by

$$\tau_p = \frac{\rho_p d_p^2}{18\mu}. \quad (9)$$

At the edge of the viscous sublayer, the particle velocity perpendicular to the wall can be approximated by (Im and Chung, 1983)

$$V_0 = V_w + \frac{u_w'}{\sqrt{Sc_p}} \quad (10)$$

where u_w' is the wall-directed fluctuating fluid velocity at the edge of the viscous sublayer, V_w is the wall-directed ballistic particle velocity, and Sc_p is the particle Schmidt number. u_w' can be estimated in terms of the friction velocity, u_τ , as $u_w' = 0.4u_\tau$ (Klewicki, 1989). The friction velocity can be calculated from the turbulent kinetic energy,

$$u_\tau = \sqrt{k\sqrt{C_\mu}} \quad (11)$$

The particle Schmidt number represents the ratio of the fluid eddy diffusivity to the particulate eddy diffusivity and can be written (Im and Chung, 1983)

$$Sc_p^{-1} = 1 + \frac{\exp\left(-\frac{\tau_f}{\tau_p} + 1\right) - 1}{1.72\left[\left(\frac{\tau_f}{\tau_p}\right)^2 - 1\right]} \quad (12)$$

where τ_p is the particle relaxation time given by Eq. 9. τ_f is the turbulence time scale and is of the order of the fluctuation time of large eddies in the buffer region. Assuming the thickness of the buffer region to be about 24 dimensionless wall units and the characteristic buffer region fluctuating velocity to be $u_w' = 0.4u_\tau$ (Klewicki, 1989),

$$\tau_f = \frac{24\nu}{0.4u_\tau^2} \quad (13)$$

where ν is the fluid kinematic viscosity. Accounting for the particle radius, a non-dimensional effective stop distance can be written in terms of wall coordinates as

$$S^+ + r^+ = \frac{\left(S + \frac{d_p}{2}\right)u_\tau}{\nu} \quad (14)$$

where d_p is the particle diameter and S is determined with Eq. 8 to Eq. 14.

The flux of particles through the buffer region and viscous sublayer to the wall can be determined from the expression

$$J = (D_p + \varepsilon_p) \frac{dC}{dy} \quad (15)$$

where D_p and ε_p are Brownian and eddy diffusivities of the particles, respectively, C is the particle concentration and y is the coordinate direction perpendicular to the wall.

Defining a deposition velocity by

$$V_D = \frac{J}{C_0} \quad (16)$$

where C_0 is the particle concentration outside the buffer region, Eq. 15 can be non-dimensionalized in terms of wall coordinates and C_0 as

$$V_D^+ = \left(\frac{D_p}{\nu} + \frac{\varepsilon_p}{\nu} \right) \frac{dC^+}{dy^+} \quad (17)$$

This equation is rearranged and integrated from the edge of the buffer region to one effective stop distance from the surface as

$$\frac{1}{V_D^+} \left[\int_{C^+(S^+ + r^+)}^{C^+=1} dC^+ \right] = \int_{(S^+ + r^+)}^6 \frac{dy^+}{\left(\frac{D_p}{\nu} + \frac{\varepsilon_p}{\nu} \right)} + \int_6^{30} \frac{dy^+}{\left(\frac{D_p}{\nu} + \frac{\varepsilon_p}{\nu} \right)} \quad (18)$$

In Eq. 18, it is assumed that $S^+ + r^+ < 6$; for the case where $S^+ + r^+ > 6$, the left term on the right hand side of Eq. 18 disappears and the limits of integration of the right term become $S^+ + r^+$ and 30. The particle eddy diffusivity can be determined from the fluid eddy diffusivity and the particle Schmidt number as

$$\varepsilon_p = \frac{\varepsilon}{Sc_p} \quad (19)$$

The fluid eddy diffusivity for the buffer region can be calculated from (Im and Chung, 1983)

$$\varepsilon = 0.4u_\tau(y + k_s) \left(1 - \exp\left(-\frac{(y + k_s)}{A} \right) \right)^2, \quad 6 \leq y^+ \leq 30 \quad (20)$$

where $A = 26$ and k_s is the surface roughness. Eq. 20 is used to determine ε_p in the right term on the right hand side of Eq. 18. In the viscous sublayer, the eddy diffusivity can be evaluated from (Davies, 1945)

$$\varepsilon = \left(\frac{y}{C_1} \right)^3, \quad 0 \leq y^+ \leq 6 \quad (21)$$

where the constant C_1 is evaluated with the condition that Eq. 20 and Eq. 21 match at the edge of the viscous sublayer ($y^+ = 6$). Eq. 21 is used to determine ε_p in the left term on the right hand side of Eq. 18. The Brownian diffusivity is given by (Shimada et al., 1993)

$$D_p = \frac{\kappa T C_c}{3\pi\mu d_p} \quad (22)$$

where κ is the Boltzmann constant, T and μ are the fluid temperature and viscosity, respectively. The Cunningham correction factor, C_c , in Eq. 22 can be expressed as (Davies, 1945)

$$C_c = 1.0 + Kn \left(1.257 + 0.4 \exp\left(\frac{-1.1}{Kn} \right) \right) \quad (23)$$

where the Knudsen Number, Kn , is the ratio of the ratio of the molecular mean free path, λ , to the particle radius. The molecular mean free path can be determined from (Davies, 1945)

$$\lambda = \frac{\mu}{0.499\rho_f\bar{c}} \quad (24)$$

where the average molecular speed, \bar{c} , is given by

$$\bar{c} = \sqrt{\frac{8P}{\pi\rho_f}} \quad (25)$$

assuming an ideal gas. The Cunningham correction factor provides a correction for the fluid drag on a sphere in the slip flow regime, i.e, when the sphere diameter is of the order of the molecular mean free path.

Turbulent Particle Deposition

Using Eq. 19 and Eq. 21 in the integration of the first term on the right hand side of Eq. 18 yields for the viscous sublayer

$$I_{vs} = \int_{S^+ + r^+}^6 \frac{dy^+}{\left(\frac{D_p}{v} + \frac{\epsilon_p}{v}\right)} = C_1 S c_p^{1/3} \left(\frac{v}{D_p}\right)^{2/3} \left[\frac{1}{6} \ln \frac{(1+\phi)^3}{1+\phi^3} + \frac{1}{\sqrt{3}} \tan^{-1} \frac{2\phi-1}{\sqrt{3}} \right]_{\phi_1}^{\phi_2} \quad (26)$$

where $\phi = \frac{y^+}{C_1} \left(\frac{v}{D_p S c_p}\right)$

Using Eq. 20 and Eq. 21 in the integration of the second term on the right hand side of Eq. 18 yields for the buffer region

$$I_{br} = \int_6^{30} \frac{dy^+}{\left(\frac{D_p}{v} + \frac{\epsilon_p}{v}\right)} = 2.5 S c_p \left\{ 0.92 \ln \frac{30 + k_s^+}{5 + k_s^+} - 0.5 \left(\frac{A^+}{30 + k_s^+} - \frac{A^+}{5 + k_s^+} \right) - 0.54 \left[\left(\frac{A^+}{30 + k_s^+} \right)^2 - \left(\frac{A^+}{5 + k_s^+} \right)^2 \right] \right\} \quad (27)$$

Substituting Eq. 26 and Eq. 27 into Eq. 18, integrating, and rearranging yields

$$V_D^+ = \frac{1 - C_{S^+ + r^+}^+}{I_{vs} + I_{br}} \quad (28)$$

where I_{vs} and I_{br} are determined by Eq. 26 and Eq. 27, respectively. At a distance $S^+ + r^+$ from the wall,

$$C_{S^+ + r^+}^+ = \frac{V_D^+}{(V_0^+)_{S^+ + r^+}} \quad (29)$$

where V_0^+ is the dimensionless wall directed component of the particle velocity, so Eq. 29 can be re-written

$$V_D^+ = \frac{1}{I_{vs} + I_{br} + \frac{1}{(V_0^+)_{S^+ + r^+}}} \quad (30)$$

In the absence of thermophoresis, the deposition velocity is determined from Eq. 30, then the flux of particles to the wall is calculated from Eq. 16.

Thermophoresis

When a particle lacks sufficient inertia to penetrate the viscous sublayer, an external force must act if the particle is to impact the surface adjacent to the boundary layer. In the presence of a thermal gradient, such a force may arise from an asymmetric interchange of momentum between a particle and the surrounding gas molecules, driving the particle in the direction opposite the thermal gradient. The magnitude of this thermophoretic force is largely a function of the Knudsen number, the temperature gradient, and the particle radius. Through integration of the gas molecule/particle momentum interchange over the surface of the particle, Jacobsen and Brock (1965) have determined an expression for the thermophoretic force for Knudsen numbers somewhat less than 1,

$$F_T = -3\pi\mu d_p^2 \left(\frac{c_{tm}Kn \left\{ \left(\frac{k_f}{k_p} + c_tKn \right) \left(1 + \frac{4}{3}ac_mKn \right) - \frac{4}{3}ac_mKn \right\}}{(1 + 3c_mKn) \left(1 + 2\frac{k_f}{k_p} + 2c_tKn \right)} \right) \nabla T \quad (31)$$

where k_f and k_p are the thermal conductivities of the gas and particles, respectively; the temperature jump coefficient is given by $c_t = 3.32$; the thermal velocity coefficient is given by $c_{tm} = 0.461$; $c_m = 1.19$; and $a = 2.4$. Equating the thermophoretic force to a Stokes drag gives a thermophoretic deposition velocity,

$$V_T^+ = \frac{F_T C_c}{12\pi\mu d_p} \quad (32)$$

When a thermophoretic force is present, Brownian diffusion will have relatively little impact on the rate of particle migration across the laminar sublayer (Byers and Calvert, 1967), so in this case Eq. 30 becomes

$$V_D^+ = \frac{1}{I_{br} + \frac{1}{V_T^+}} \quad (33)$$

and again a deposition velocity can be determined.

Results and Discussion

Measurements of both isothermal and thermophoretic deposition for flow in circular tubes have been made in laboratory settings. The deposition model described above has been evaluated through simulations of these experiments.

Measurements of the isothermal deposition of iron particles ($\rho=7840 \text{ kg/m}^3$) in circular tubes have been made by Friedlander and Johnstone (1957). These data are compared to numerical predictions of deposition in Figure 1; the numerical predictions agree well with the experimental data. Deposition increases with the tube Reynolds number, since increased turbulence intensity imparts a higher wall directed velocity to the particles. Deposition rates for $1.57 \mu\text{m}$ particles are higher than those for $0.8 \mu\text{m}$ particles in the same size tube, since the larger particles have higher inertia and are more likely penetrate the laminar sublayer. At some point, further increases in particle diameter may result in decreasing deposition when the large particles become less likely to be entrained by the turbulence and directed towards the wall. However, this behavior is not seen in these particles.

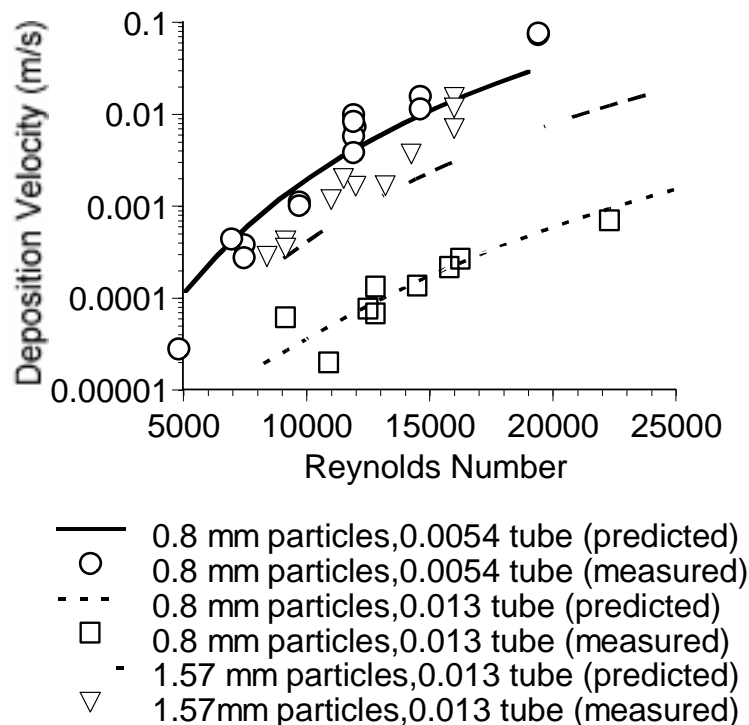


Figure 1. Comparison of predicted and measured (Friedlander and Johnstone, 1957) values of isothermal deposition of iron particles ($\rho=7840 \text{ kg/m}^3$) of various diameters in circular tubes as a function of Reynolds number.

Predictions of isothermal deposition of uranine-methylene blue ($\rho=1500 \text{ kg/m}^3$) are compared to experimental data (Sehmel, 1968) in Figure 2 and Figure 3. Once again, both predicted and measured deposition rates increase with tube Reynolds number and particle diameter, as shown in Figure 2. Deposition velocity is plotted as a function of particle diameter in Figure 3. Both the numerical predictions and experimental data indicate increasing deposition with increasing particle diameter over most of the range of particle sizes, since the larger particles are more likely to have sufficient inertia to penetrate the viscous sublayer. However, the experimental data shows a leveling off and decrease in deposition for the largest particles which is not predicted by the numerical scheme for the same size particles. The leveling off and decrease in deposition occurs when particles are less likely to be entrained by the turbulence. Apparently, the numerical scheme overpredicts the effect of the flow field on these largest particles.

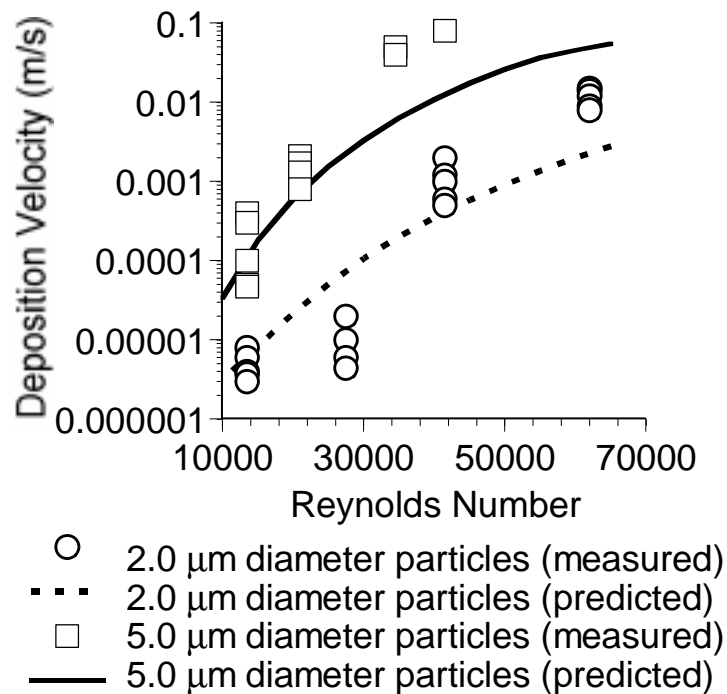


Figure 2. Comparison of predicted and measured values (Sehmel, 1968) of isothermal deposition of uranine-methylene blue particles of various diameters in a 0.0293 m diameter tube as a function of Reynolds number.

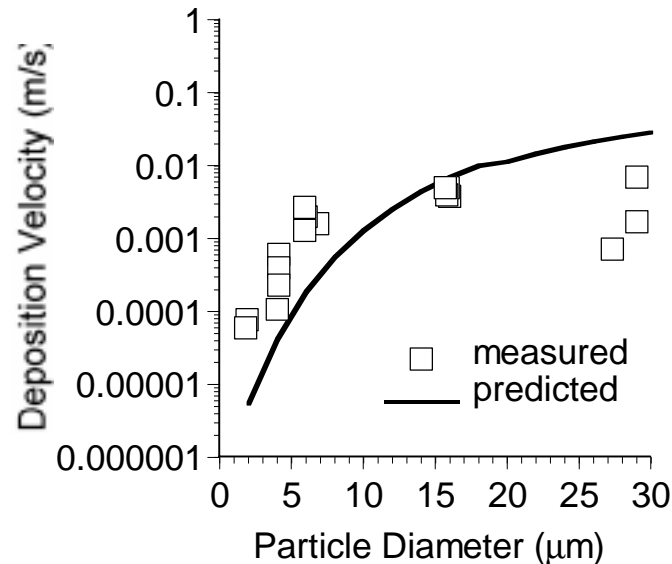


Figure 3. Comparison of predicted and measured (Sehmel, 1968) values of isothermal deposition of uranine-methylend blue particles ($\rho=1500 \text{ kg/m}^3$) in a 0.0713 m diameter tube ($Re=36000$) as a function of particle diameter.

Numerical predictions of thermophoretic deposition of NaCl particles in a 0.00792 m diameter tube are compared to the experimental data of Byers and Calvert (1969) in Figure 4 and Figure 5. Hot aerosol entered the tube at a specified temperature while the cooler tube walls were maintained at 300K. Figure 4 shows deposition efficiency, or the fraction of particles injected that are deposited, plotted as a function of particle diameter for various flow temperatures. Both the experimental data and the numerical predictions indicate that deposition is highest for higher temperature aerosols, when the thermophoretic force is largest, and for smaller particles. At the highest aerosol inlet temperature of 755.5K, the numerical predictions closely follow the experimental measurements over the range of particle diameters considered. For lower aerosol temperatures, the numerically predicted deposition is lower than the experimental data for the largest particles.

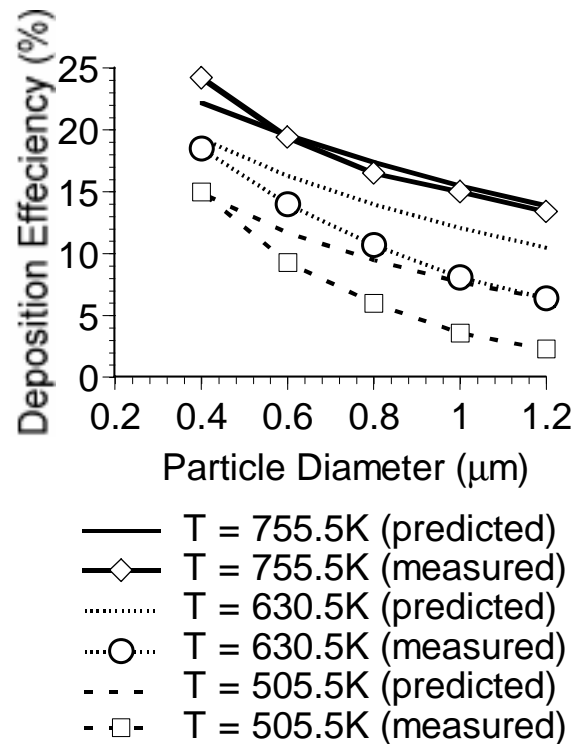


Figure 4. Comparison of predicted and measured (Byers and Calvert, 1969) values of thermophoretic deposition of NaCl particles in a 0.00792 m diameter tube for various flow temperatures as a function of particle diameter.

The effect of tube length on thermophoretic deposition is shown in Figure 5. It can be expected that deposition efficiency will increase with increasing tube length, but the increase may not be linear since the aerosol will cool in longer tubes, decreasing the thermophoretic force. This behavior is shown by both the experimental data and the numerical predictions in Figure 5. For the shortest tube ($L/D=38.5$), the numerical predictions fairly closely follow the experimental data. For longer tubes, however, the agreement is not as good; the numerical scheme overpredicts deposition. This could be due to either heating of the cooling water in the experimental apparatus or underprediction of heat transfer to the tube walls in the numerical scheme.

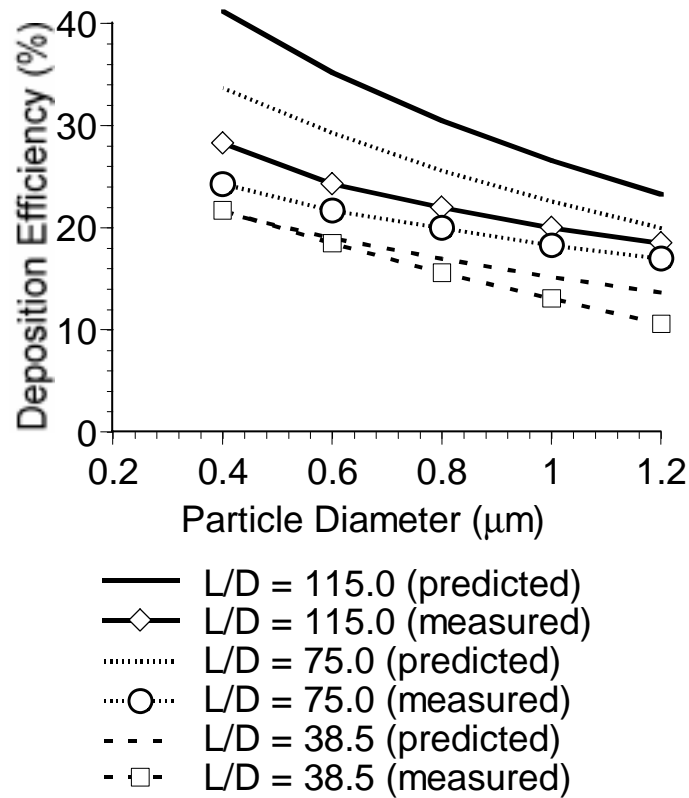


Figure 5. Comparison of predicted and measured (Byers and Calvert, 1969) values of thermophoretic deposition of NaCl particles in a 0.00792 m diameter tube for various pipe length/diameter (L/D) in a 0.00792 m diameter tube for various pipe length/diameter (L/D).

Conclusion

In summary, a deposition model has been coupled with a particle cloud tracking technique and has been evaluated through comparison of numerical predictions with experimental data for circular tubes. The scheme has been shown to reasonably predict both isothermal and thermophoretic particle deposition. Although the test cases have been circular tubes, the numerical method is not limited to such geometries, and should be applicable to arbitrary geometries.

References

- Baxter, L.L., "Turbulent Transport of Particles," Ph.D. Dissertation, Department of Chemical Engineering, Brigham Young University, Provo, Utah (1989).
- Crowe, C.T., Sharma, M.P., and Stock, D.E., "The Particle-Source-in-Cell Method for Gas and Drop-let Flow," *J. Fluids Eng.*, **99**, 325 (1977).
- Byers, R.L. and Calvert, S., "Particle Deposition from Turbulent Streams by Means of Thermal Force," *I&EC Fundamentals*, **8** 1969.
- Davies, C.N., "Definite Equations for the Fluid Resistance of Spheres," *Proc. Phys. Soc.*, **57**, 18 (1945).
- Friedlander, S.K. and Johnstone, H.F., "Deposition of Suspended Particles from Turbulent Gas Streams," *Ind. Eng. Chem.*, **49**, 1151 (1957).
- Im, K.H., and Chung, P.M., "Particulate Deposition from Turbulent Parallel Streams," *AIChE J.*, **29**, 498 (1983).
- Jain, S., "Three-Dimensional Simulation of Turbulent Particle Dispersion Applications," Ph.D. Dissertation, Department of Chemical and Fuels Engineering, University of Utah (1996).
- Jacobsen, S. and Brock, J.R., "The Thermal Force on Spherical Sodium Chloride Aerosols," *J. Colloid Sci.*, **20**, 544 (1965).
- Klewicki, J.C., "On the Interactions Between the Inner and Outer Region Motions in Turbulent Boundary Layers," Ph.D. Dissertation, Department of Mechanical Engineering, Michigan State University (1989).
- Shuen, J.S., Chen, L.D. and Faeth, G.M., "Evaluation of a Stochastic Model of Particle Dispersion in a Turbulent Round Jet," *AIChE J.*, **29**, 167 (1983).
- Shimada, M., Okuyama, K., and Asai, M., "Deposition of Submicron Aerosol Particles in Turbulent and Transitional Flow," *AIChE J.*, **39**, 17 (1993).
- Wallis, G.B., "One-Dimensional Two-Phase Flow," McGraw-Hill, New York (1969).
- Wang, L.P., "On the Dispersion of Heavy Particles by Turbulent Motion," Ph.D. Dissertation, Washington State University (1990).